MANUSCRIPT REPORT FORM

PAPER NUMBER (if known): **632 in** A2-2-8

TITLE OF PAPER: The Effect of Cycle Frequency, H_2O and CO_2 on TBC Lifetime with NiCoCrAlYHfSi Bond Coatings

CORRESPONDING AUTHOR: Michael J. Lance

FULL MAILING ADDRESS: 1 Bethel Valley Rd., MS 6064, Oak Ridge, TN 37831-6068, USA

TELEPHONE: 865-241-4536

FAX: 865-574-6098

E-MAIL: lancem@ornl.gov

The Effect of Cycle Frequency, H_2O and CO_2 on TBC Lifetime with NiCoCrAlYHfSi Bond Coatings

M. J. Lance, K. A. Unocic, J .A. Haynes and B. A. Pint

Materials Science and Technology Division

Oak Ridge National Laboratory, 1 Bethel Valley Rd., Oak Ridge, TN 37831, USA

Furnace cycle testing of superalloy 1483 and X4 substrates with high velocity oxygen fuel (HVOF) NiCoCrAlYHfSi bond coatings and air plasma sprayed (APS) yttria-stabilized zirconia (YSZ) top coatings were conducted at 1100 °C in various environments. Average thermal barrier coating (TBC) lifetimes were 5-6 times longer when 100 h cycles were used to simulate base-load power generation operation, compared to the 1 h aero-engine standard cycle. Longer exposure times for 100 h cycles increased the interdiffusion resulting in no clear effects of H_2O and CO_2 additions on average TBC lifetime for the 1483 substrates, contrary to the results with 1 h cycles where the addition of H_2O reduced TBC lifetime. The lower Al content and perhaps the higher Ti content in 1483 compared to X4 resulted in lower TBC lifetimes for 1483. Photo-stimulated luminescence piezospectroscopy (PLPS) and 3D microscopy were used to measure residual stress in the alumina scale and surface roughness, respectively, on specimens with and without a YSZ top coating.

Keywords: photo-stimulated luminescence piezospectroscopy (PLPS); water vapor; bond coating; alumina scale; TBC

1. Introduction

Along with low natural gas prices, increased emissions regulation in the U.S. have resulted in the closure of many smaller, older coal-fired power plants and less utilization of the entire fleet in the past 7 years [1]. When new U.S. coal-fired generation is built, new technology will be required to reduce Hg, SO_x, NO_x and CO_2 emissions. As part of this trend, two commercial scale (~600 MW) integrated gasification combined cycle (IGCC) plants have recently been built in the U.S., one with >60% CO_2 capture and the other capture ready. These plants burn coal-derived synthesis gas (syngas) in turbines that are very similar to natural gas combined cycle (NGCC) plants with turbine exhaust generating steam in the bottoming cycle. One drawback of IGCC is that syngas-fired turbines are de-rated (i.e. fired at a lower maximum temperature than similar NGCC turbines), which reduces the turbine efficiency resulting in lower plant electricity output for the same amount of fuel [2].

Improved materials/coatings may enable a reduction in the de-rating; however, it is critical to understand the syngas turbine environment as well as other innovative concepts that may contain high levels of CO_2 and/or H_2O. While sulfur or ash contamination from gasifying coal could be mitigated, especially by carbon capture processes applied to the syngas prior to combustion, the higher water vapor content (compared to NGCC) is determined by the fuel (ranging from syngas to pure H_2) and combustion conditions [2, 3]. Increasing the CO_2 in the turbine exhaust could facilitate CO_2 capture [4].

Another trend for both NGCC and IGCC is the increased use of less expensive superalloys for power generation turbines. Eliminating Re from superalloys reduces alloy costs by ~30% and the highest performance superalloys may not be needed as temperatures are lower in these turbines in order to achieve the 3-5 year overhaul time before stripping and reapplying the thermal barrier coating (TBC). Furthermore, 1st generation single crystal superalloys like

Re-free 1483 [5] offer higher Cr contents yielding better hot corrosion resistance than 2nd generation alloys like X4 (3% Re) [6, 7].

These IGCC-relevant factors have been combined in this study in order to evaluate where new materials might be beneficial. The effects of water vapor on high temperature oxidation have been widely studied in the past 15 years [8-16], including alumina-forming alloys and TBC bond coatings but a complete understanding has yet to be clarified. Advanced characterization techniques also are being employed, such as photo-stimulated luminescence piezospectroscopy (PLPS) to measure stress in alumina scales [17-20]. The technique is based upon the correlation of stress to the frequency shift of the R-lines produced by Cr^{3+} in Al_2O_3 [21]. The signal intensity is large enough to allow for non-destructive stress measurement from the scale grown under a YSZ (yttria stabilized zirconia) top coat [22]. In this work, PLPS is used to characterize specimens with and without a APS-YSZ top coating to build upon previous work [23-25].

2. Material and methods

Superalloy coupons of X4 and 1483, 2mm thick and ~16mm diameter were coated using a commercial-type HVOF process with commercial NiCoCrAlYHfSi [26] (Table I) powders at Stonybrook Univ. The HVOF-coated specimens were annealed in a vacuum of 10^{-4} Pa for 4h at 1080 °C and had a bond coating thickness of ~100 µm. A ~200 µm-thick APS YSZ layer was then applied on one side using standard conditions.

For each condition, 4-6 specimens were evaluate d: 3-5 with YSZ and one without YSZ to study the surface morphology evolution. For 1 h cycles at 1100 °C, specimens were hung by a Pt-Rh wire in an automated cyclic rig with a controlled environment and then cooled in laboratory air for 10 min for each cycle. For 100 h cycles, specimens were placed in an alumina boat, heated to temperature over ~4 h in flowing argon and furnace cooled after the cycle.

Environments included (1) dry air, (2) air with 10±1% or 50±2% vol.%H_2O and (3) buffered 90%(CO_2-0.15%O_2)+10%H_2O [16, 27]. The injected water was measured to calibrate its concentration. Mass change was measured using a Mettler-Toledo model XP205 balance.

Periodically during exposure, specimens were examined using scanning electron microscopy (SEM) equipped with an energy dispersive x-ray spectrometer (EDS), a Keyence VHX digital microscope and optical profiler [24], and a Dilor XY800 Raman microprobe (Horiba Scientific, Edison, NJ) with an Innova 308c Ar^+ laser (Coherent, Inc., Santa Clara, CA) operating at 5145 Å with a power at the scale surface of 2.5 mW. PLPS stress maps were collected from the same 500 x 670 μm region as the digital images where average roughness (R_a) was calculated from the height maps [24, 25].

The laser spot size and the mapping step size were both 10 μm and the acquisition time for one spectrum was 0.1 s. A total of 3468 spectra were collected for each map. Since the bond coat surface is not flat and the scale is often cracked, the stress state was not assumed to be biaxial and so hydrostatic stress (the average of the trace of the stress tensor) was determined by dividing the frequency shift of the R2 line from a zero stress reference (NIST standard reference material 676A) by 7.61 cm^{-1}/GPa [21]. Owing to the large number of spectra collected no attempt was made to deconvolute multiple stress states and only a single stress (one set of R-lines) was fitted to each spectrum. One YSZ-coated specimen was also mapped using the same procedure described above with a fiducial marker cut into the YSZ top coating to locate the area. In order to improve the signal intensity, the laser power and the acquisition time were increased to 10 mW and 1 s, respectively. Fig. 1 shows typical spectra acquired from the YSZ-coated specimen and the bare bond coat specimen after 100 h in air with 50 vol% H_2O at 1100 °C and the zero-stress reference powder. The intensity of the spectrum measured underneath the YSZ was ~10,000 times weaker than that measured on the scale on the bare bond coating. As noted by others [28,

29] this decline in intensity is due to attenuation of both the incident and luminescent light by the YSZ layer. After 5 x 100 h cycles, spalled Al_2O_3-containing scale debris on the YSZ surface obscured the results but debris after 10 x 100h cycles was removed using compressed air. After YSZ-coating failure (near 100% spall in all cases), the specimens were metallographically sectioned and examined by light microscopy and electron probe microanalysis (EPMA) using a JEOL model 8200 microprobe.

3. Results and discussion

Fig. 2 summarizes the average TBC lifetime data using both 1 h [25, 30] and 100 h cycles at 1100 °C. The lifetimes are the average of three coated specimens except for the 1483 specimens exposed in 100 h cycles where five specimens were exposed. For reference, data from an earlier study with a lower roughness bond coating (Ra~5) are also included [27]. The substrate is marked X4+ as it also contained 1–2 ppma Y and 2–3 ppma La. The same commercial bond coating powder was used in each case. As reported previously [25, 30], the lifetimes in 1 h cycles indicated (1) the increased bond coating roughness did not increase the average lifetime, (2) the TBC lifetime on 1483 substrates was lower than with the X4 substrates with bond coatings made in the same batch and (3) the addition of 10% H_2O decreased the TBC lifetime compared to dry air and increasing to 50% H_2O further reduced the lifetime. The result with 10% H_2O was consistent with a previous study but in that study with Ra~5 bond coatings, cycling with 50% H_2O caused no further decrease in lifetime [27].

As expected, the average TBC lifetimes were much higher when the cycle frequency was increased to 100 h to better simulate a base load power generation duty cycle. Some of the coatings on the X4+ substrate lasted 10X the 1 h cycles and were not reported previously [27]. As noted previously [25], the rougher (Ra~8) bond coatings were inadvertently thinner than the

Ra~5 bond coatings and this is the likely reason for the drop in average TBC lifetime from 3733 h to 2200 h with the X4-type substrates (see Fig. 2). The longer-lasting smoother bond coatings also failed gradually by edge delamination that was detected by thermography while the rougher bond coatings spalled completely at failure. Previously, the Y and La additions in X4+ did not appear to produce any beneficial effects on TBC lifetime in 1 h cycles [27]. Consistent with the 1 h cycles, the average TBC lifetime with 10% H_2O was substantially lower for the coatings on 1483 substrates compared to the X4 substrates. These specimens were all coated in the same batch and were tested at the same time. Not consistent with the 1 h cycles was the inconsistent effect of environment on the average TBC lifetimes with the 1483 substrates. The specimens tested in laboratory air had the shortest average lifetime of 860 h, while those tested with 10% H_2O had the longest average TBC lifetime of 1360 h. A 1040 h average lifetime was observed with 50% H_2O. For this study, a new environment containing 90% buffered CO_2 with 10% H_2O was added and exhibited an average lifetime of 1120 h.

Characterization of the specimens exposed with 1 h cycles was reported previously (except for those exposed in 50% H_2O) [25] so the characterization will focus on the specimens cycled with 100 h cycles. Fig. 3 shows the surface roughness as a function of exposure time for the specimens without a YSZ top coating. The higher bond coating roughness in this batch of specimens was achieved by over spraying with coarser powder of the same composition, which resulted in a surface morphology like that shown in Fig. 4 with large intermittent spherical particles. With exposure, all of the samples initially increased in roughness due to oxidation followed by a decrease due to the spallation of some spherical particles as they were undercut by oxidation [25]. The exception to this trend was the coating exposed for 10 x 100 h cycles in 50% H_2O, which continued to increase in roughness. Further inspection of the region examined

on this specimen showed spallation from a valley that effectively increased the roughness measurement despite a similar behavior.

For comparison, the specimen exposed to 1 h cycles and 50% H_2O exhibited a more rapid increase and decrease in roughness because of the much larger number of thermal cycles experienced (500) compared to 10 cycles for the other specimens. The roughness of the YSZ-coated specimen exposed to 100 h cycles and 50% H_2O is also shown in Fig. 3. The roughness did not change during exposure in contrast to prior results for EB-PVD YSZ top coatings with a Pt-modified aluminide bond coating exposed to 1 h cycles [31]. After YSZ spallation, the roughness of the bond coating on this sample was significantly lower as many of the spherical particles remained embedded in the adjacent YSZ at failure.

The stress measurements are shown in histograms in Fig. 5 after 100 and 1000 h. Surprisingly, the specimen exposed in 10% H_2O and 100 h cycles without a bond coating consistently had the lowest stress at both times, even lower than the specimen exposed in 1 h cycles which had already experienced 100 cycles after 100 h of exposure, Fig. 5a. The other three specimens without bond coatings exposed in 100 h cycles all exhibited a broad stress distribution after 1 cycle. At longer times, the compressive stress distribution narrowed with the peak distribution of 0.1 GPa after 5 cycles caused by extensive cracking, which relieved stress in the scale. The final stress measurement after 10 cycles is shown in Fig. 5b where the distribution skewed towards higher stresses due to new scale formation. New scale growth on the specimen cycled for 500, 1-h cycles in 50% H_2O resulted in a small peak at 4 GPa (not shown).

The most unique distribution in Fig. 5 was the stresses measured from the specimen with a YSZ top coating exposed in 100 h cycles and 50% H2O. The 0.8 GPa peak stress was significantly narrower than many of the other specimens whose peak was at only 0.1 GPa, Fig. 5a. The higher stress in the scale may be caused by the increased constraint imposed on the scale

by the YSZ layer [32]. Furthermore, the peak did not change significantly between 1 and 10 cycles, Fig. 5b, surprisingly because the YSZ coating spalled after the next cycle. After spallation, the stress histogram of the exposed bond coating surface was similar to those measured for the bare bond coatings samples in Fig. 5b. These results suggest that measuring the residual stress beneath the YSZ top coating may be more useful than studying HVOF-coated specimens without a top coating.

Fig. 6 shows examples of the stress maps collected on specimens exposed in 100 h cycles in 50% H_2O with and without a YSZ top coating. As observed with 1 h cycles [25], the scale formed on the spherical particles (as shown in Fig. 4) cracks more readily than the scale in the flatter regions due to out-of-plane tensile stresses generated during cooling. These particles correspond to the round, low-stress regions on the bare bond coating after 1 cycle, Fig. 6a. Stress relief associated with these particles can also be observed at the interface through the YSZ coating after the same exposure time, Fig. 6c. Compared to the bare bond coating, fewer low stress regions were observed, suggesting that the YSZ layer inhibited scale cracking after 1 cycle, consistent with stress distributions in Fig. 5a. After 10 cycles, the bare bond coating had more near-zero stress regions suggesting that more of the remaining scale was cracked. However, some areas had stresses exceeding 2 GPa, which is attributed to new adherent scale growth on the spalled regions, Fig. 6b. In contrast, the stress in the scale under the YSZ layer in Fig. 6d was mostly intact (~0.8 GPa) but the zero-stress regions increased after 10 cycles. Again, this is consistent with the histrogram for this data in Fig. 5b.

It is well-known that the YSZ layer will increase the laser spot size at the thermally-grown scale due to light dispersion within the YSZ with estimates ranging from 20 μm [33-35] to 160 μm [29]. One factor that may improve the spatial resolution is the increased R-line signal from cracked scale [25, 36]. The low stress regions under the YSZ in Fig. 6c emitted >10 times

more luminescence than the surrounding high stress regions. Cracked scale will thus contribute more of the luminescence to the measured spectrum thereby allowing features that may be much smaller than the illuminated spot to appear in the stress maps.

Fig. 7 shows cross-sectional images of representative failed YSZ-coated specimens. As expected, the rougher bond coating caused the interfacial crack to travel mainly through the YSZ layer but included peaks of the spherical particles where thicker Ni-rich oxide formed. The failure was not significantly different between 1 and 100 h cycles in 50%H_2O, Figs. 7a and 7b. One difference between the 1 and 100 h cycle specimens is the oxides formed at the interface between the bond coating and the 1483 substrate. With the longer exposure time (240 x 1 h cycles vs. 11 x 100 h cycles), the oxides appear to have grown significantly, they are clearly evident in the dark field image in Fig. 7d. Often discrete oxide particles at this interface are attributed to embedded grit from roughening of the substrate prior to coating. However, in these specimens, the interfacial particles are clearly growing with exposure time and their formation is attributed to the relatively poor oxidation resistance of uncoated 1483 compared to X4. The spray coating process does not perfectly coat the coupon edge and this can lead to some ingress of oxygen along this interface from the edge. Fig. 8 shows an extreme case where the bond coating began to lift off at the coating-substrate interface after 10 x 100 h cycles in 10% H_2O.

A cross-section is shown from the CO_2-H_2O environment in Figs. 7c and 7d, which showed no indication of any internal oxidation/carburization due to this environment. It appears that replacing air with buffered CO_2 in this experiment did not have a significant detrimental effect. A companion study with aluminide bond coatings and EB-PVD top coatings using 1 h cycles at 1150 °C in the same environments found a longer lifetime in CO_2+10% H_2O than in air +10% H_2O [30]. Relatively little prior work has been performed on alumina-forming coatings or alloys in CO_2-containing environments at high temperature. A 1965 study of type 304 stainless

steel found internal carburization in 1 bar CO_2 but more protective behavior for FeCrAl alloys [37].

The prior study of coated 1483 in 1h cycles found significantly greater interdiffusion on these coatings compared to X4 substrates [25], which was attributed to the lower Al content in 1483. With the longer exposure times in 100 h cycles, this issue is likely to be even more severe. Fig. 9 shows EPMA line profiles from one of the YSZ-coated 1483 specimens exposed for 1400 h in air with 10% H_2O. The Al content has dropped to ~4 wt%, near the same level as the substrate (3.4%) and significantly below the 12.3% in the starting coating powder. The other significant change is that there is now more than 1.5% Ti that has diffused in from the 1483 substrate. While it has been previously established that 0.3% Ti does not appear to significantly affect oxide adhesion on NiCrAlYHf model alloys [38], such a high level of Ti may cause a detrimental effect. Thus, one reason that TBC lifetime appeared to be relatively unaffected by environment for the 100 h cycle samples on 1483 may be that the bond coating becomes so severely depleted in Al at these long exposure times that this effect leads to failure.

While 1100 °C was selected to accelerate TBC failures to reasonable times, this temperature is particularly high for 1483 without a coating. The low level of Al and high Ti content result in very poor oxidation resistance especially compared to X4 [39]. The disk specimen geometry resulted in edges that were not fully coated. While this was not an issue for X4, it appears to be an issue for 1483. The liftoff shown in Fig. 8 could cause the YSZ coating to fail as well. The susceptibility of uncoated 1483 to rapid oxidation is also a concern as the bond coating was not as thick as in the previous study [27]. Thus, when evaluating less oxidation resistance substrates, more care may be needed to coat the entire specimen or the coating temperature may need to be reduced. However, reducing the temperature to 1050 °C would likely

greatly increase the coating lifetime but is still not a low enough temperature for uncoated 1483 to form a protective oxide, especially in the presence of water vapor [39].

4. Conclusion

Furnace cycling testing of HVOF NiCoCrAlYHfSi bond coatings and APS YSZ top coatings was conducted at 1100 °C with variables relevant to current land-based, syngas-fired gas turbines: (1) different environments, (2) different superalloys and (3) longer thermal cycles. Average TBC lifetime with 100 h cycles increased 5-6 times compared to previous testing with 1 h cycles of coatings made in the same batch. Based on the observation that additions of H_2O and CO_2 had no clear effects on the average TBC lifetime of coated 1483 substrates, these longer exposure times appear to have changed the failure mechanism to interdiffusion and increased formation of oxide at the coating-substrate interface thereby raising the concern that a specimen geometry effect may also be contributing to the failure with the less oxidation-resistant 1483 substrate. Compared to X4 substrates with the same coating, the lifetime was 30-40% lower in both 1 and 100 h cyclic testing at 1100 °C. The lower Al content and perhaps the higher Ti content in 1483 may have contributed to this difference. Stress measurements through the YSZ top coating appeared to be a more useful characterization method than studying bare HVOF bond coatings and future work will focus on this methodology.

Acknowledgements

The authors would like to thank G. Garner, T. Lowe and T. Jordan for assistance with the experimental work at ORNL and P. F. Tortorelli for comments on the manuscript. This research was sponsored by the U.S. Department of Energy, Office of Coal and Power R&D in the Office of Fossil Energy, (R. Dennis program manager).

References

[1] B.A. Pint, JOM, 65 (2013) 1024-1032.

[2] I. Wright, T. Gibbons, International Journal of Hydrogen Energy, 32 (2007) 3610-3621.

[3] B.M. White, R.W. Ames, P. Burke, in: ASME Paper #GT2013-94609, Proc. Turbo Expo 2013, 2013.

[4] L. Ruth, Materials at High Temperatures, 20 (2003) 7-14.

[5] D.M. Shah, A. Cetel, Evaluation of PWA1483 for large single crystal IGT blade applications, in: Superalloys 2000, Warrendale, PA, 2000, pp. 295-304.

[6] A. Bennett, Materials science and technology, 2 (1986) 257-261.

[7] R. Rapp, Materials science and engineering, 87 (1987) 319-327.

[8] C. Leyens, K. Fritscher, R. Gehrling, M. Peters, W.A. Kaysser, Surface and Coatings Technology, 82 (1996) 133-144.

[9] K. Onal, M.C. Maris Sida, G.H. Meier, F.S. Pettit, Materials at high temperatures, 20 (2003) 327-337.

[10] E.J. Opila, Materials Science Forum, 461-464 (2004) 765-773.

[11] B.A. Pint, J.A. Haynes, Y. Zhang, K.L. More, I.G. Wright, Surface and Coatings Technology, 201 (2006) 3852-3856.

[12] J.L. Smialek, Materials Science Forum, 595-598 (2008) 191-198.

[13] R. Kartono, D.J. Young, Materials and corrosion, 59 (2008) 455-462.

[14] W.J. Quadakkers, J. Żurek, M. Hänsel, JOM, 61 (2009) 44-50.

[15] V. Déneux, Y. Cadoret, S. Hervier, D. Monceau, Oxidation of Metals, 73 (2010) 83-93.

[16] B.A. Pint, G.W. Garner, T.M. Lowe, J.A. Haynes, Y. Zhang, Surface and Coatings Technology, 206 (2011) 1566-1570.

[17] D.M. Lipkin, D.R. Clarke, M. Hollatz, M. Bobeth, W. Pompe, Corros. Sci., 39 (1997) 231-242.

[18] C. Mercer, D. Hovis, A.H. Heuer, T. Tomimatsu, Y. Kagawa, A.G. Evans, Surface and Coatings Technology, 202 (2008) 4915-4921.

[19] V.K. Tolpygo, D.R. Clarke, Oxidation of Metals, 49 (1998) 187-212.

[20] J.A. Haynes, M.J. Lance, B.A. Pint, I.G. Wright, Surface & Coatings Technology, 146 (2001) 140-146.

[21] Q. Ma, D.R. Clarke, J. Am. Ceram. Soc., 77 (1994) 298-302.

[22] R.J. Christensen, D.M. Lipkin, D.R. Clarke, K. Murphy, Appl. Phys. Lett., 69 (1996) 3754-3756.

[23] J.A. Nychka, D.R. Clarke, S. Sridharan, E. Jordan, M. Gell, M.J. Lance, C.J. Chunnilall, I.M. Smith, S.R.J. Saunders, R. Pillan, V. Sergo, A. Selcuk, A. Atkinson, K.S. Murphy, Surface & Coatings Technology, 163 (2003) 87-94.

[24] M.J. Lance, K.A. Unocic, J.A. Haynes, B.A. Pint, Surface and Coatings Technology, 237 (2013) 2-7.

[25] J.A. Haynes, K.A. Unocic, M.J. Lance, B.A. Pint, Surface and Coatings Technology, 237 (2013) 65-70.

[26] J.T. Demasi-Marcin, D.K. Gupta, Surface & Coatings Technology, 68 (1994) 1-9.

[27] J.A. Haynes, K.A. Unocic, B.A. Pint, Surface and Coatings Technology, 215 (2013) 39-45.

[28] K.W. Schlichting, K. Vaidyanathan, Y.H. Sohn, E.H. Jordan, M. Gell, N.P. Padture, Materials Science and Engineering A, 291 (2000) 68-77.

[29] D. Liu, O. Lord, O. Stevens, P.E.J. Flewitt, Acta Materialia, 61 (2013) 12-21.

[30] B.A. Pint, K.A. Unocic, J.A. Haynes, in: Proc. 7th Inter. Conf. on Advances in Materials Technology for Fossil Power Plants, ASM International, Materials Park, OH, 2014, in press.

[31] V.K. Tolpygo, D.R. Clarke, K.S. Murphy, Surface and Coatings Technology, 188-189 (2004) 62-70.

[32] A. Atkinson, A. Selcuk, A. Selçuk, S.J. Webb, Oxidation of metals, 54 (2000) 371-384.

[33] K.W. Schlichting, N.P. Padture, E.H. Jordan, M. Gell, Materials Science and Engineering a-Structural Materials Properties Microstructure and Processing, 342 (2003) 120-130.

[34] A. Selcuk, A. Atkinson, Materials Science and Engineering a-Structural Materials Properties Microstructure and Processing, 335 (2002) 147-156.

[35] C. Rinaldi, L. De Maria, M. Mandelli, Journal of Engineering for Gas Turbines and Power, 132 (2010) 114501-114501-114504.

[36] X. Wang, A. Atkinson, L. Chirivì, J.R. Nicholls, Surface and Coatings Technology, 204 (2010) 3851-3857.

[37] H.E. McCoy, Corrosion, 21 (1965) 84-94.

[38] K.A. Unocic, B.A. Pint, Surface and Coatings Technology, 237 (2013) 8-15.

[39] B.A. Pint (2014) unpublished work.

Table I. Chemical compositions (atomic% or ppma) determined by inductively coupled plasma analysis and combustion analysis.

Material	Ni	Cr	Al	Re	Co	W	Ta	Mo	Ti	C	Other (ppma)
X4	62.8	7.5	13.0	0.9	9.7	2.1	2.2	0.4	1.2	0.02	<3Y,270Hf,17S
1483	60.8	13.6	7.3	<	8.8	1.3	1.7	1.2	4.9	0.36	<3Y,7Hf,80Si,<1S
MCrAlYHf	41.2	16.2	22.9	<	18.4	0.01	<	<	<	0.05	3860Y,710Hf, 6500Si,3S

< Indicates below the detectability limit of <0.01%

List of figure captions

Fig. 1. Luminescence spectra acquired from samples with and without a YSZ top coating after 100 h in air with 50 vol% H2O at 1100 °C and the zero-stress reference powder.

Fig. 2. The average TBC lifetime data using both 1 h and 100 h cycles at 1100 °C measured on three coated specimens except for the 1483 specimens exposed in 100 h cycles where five specimens were exposed. The substrate marked X4+ was the same as X4 but with 1–2 ppma Y and 2–3 ppma La.

Fig. 3. The average surface roughness, R_a, as a function of time at 1100 °C (100 h cycles). One sample following 1-h cycles in 50% H_2O is included.

Fig. 4. The surface profile of a bare bond coating after 100 h in 50% H_2O with R_a~8.

Fig. 5. Stress histograms measured on specimens with and without a YSZ coating after 100 h (a) and 1000 h (b) at 1100 °C.

Fig. 6. Stress maps collected from the specimens without a YSZ top coating after 1-100 h cycle (a) and 10-100 h cycles (b) and with a YSZ top coating after 1-100 h cycles (c) and 10-100 h cycles (d). Arrows indicate the same two low-stress regions after 1 and 10-100 h cycles.

Fig. 7. Cross-sectional images of failed TBC-coated specimens after 240 1-h cycles in 50% H_2O (a), 10 100-h cycles in 50% H_2O (b), and 11 100-h cycles in 90%CO_2-10%H_2O imaged in bright-field (c) and dark-field (d) modes.

Fig. 8. SEM image of bare bond coating specimen after 10 100-h cycles in air with 10% H_2O.

Figure 9. EPMA line profiles across a failed 1483 HVOF (R_a=8)/YSZ-coated specimen at 1100 °C after 14 100-h cycles in air with 10% H_2O. The gas interface is on the left and the substrate is on the right.

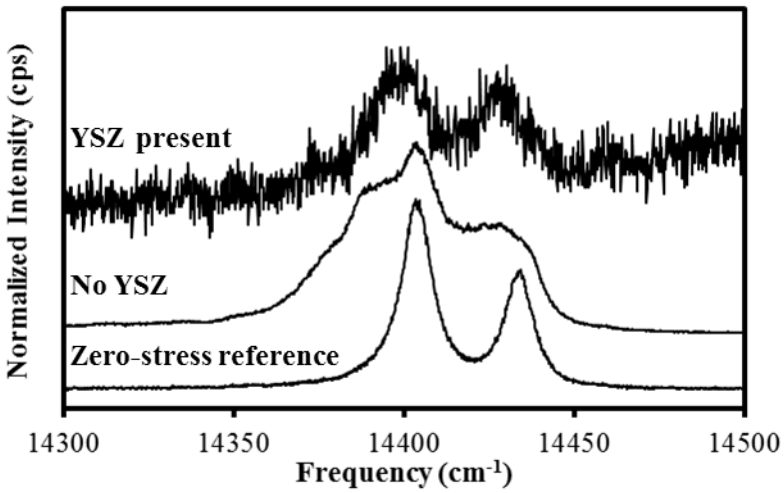
Normalized Intensity (cps)
YSZ present
No YSZ
Zero-stress reference
14300
14350
14400
14450
14500
Frequency (cm-1)

Fig. 1.

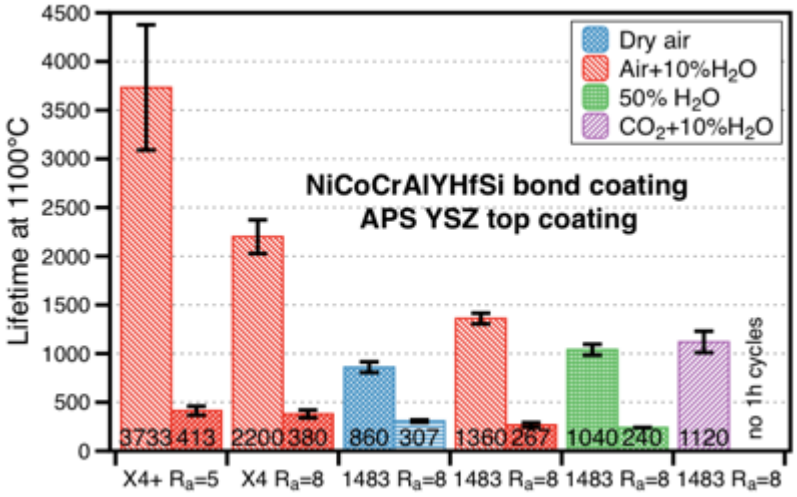
Lifetime at 1100°C
4500
4000
3500
3000
2500
2000
1500
1000
500
0
Dry air
Air+10%H2O
50% H2O
CO2+10%H2O
NiCoCrAlYHfSi bond coating
APS YSZ top coating
3733
413
2200
380
860
307
1360
267
1040
240
1120
no 1h cycles
X4+ Ra=5
X4 Ra=8
1483 Ra=8
1483 Ra=8
1483 Ra=8
1483 Ra=8

Fig. 2.

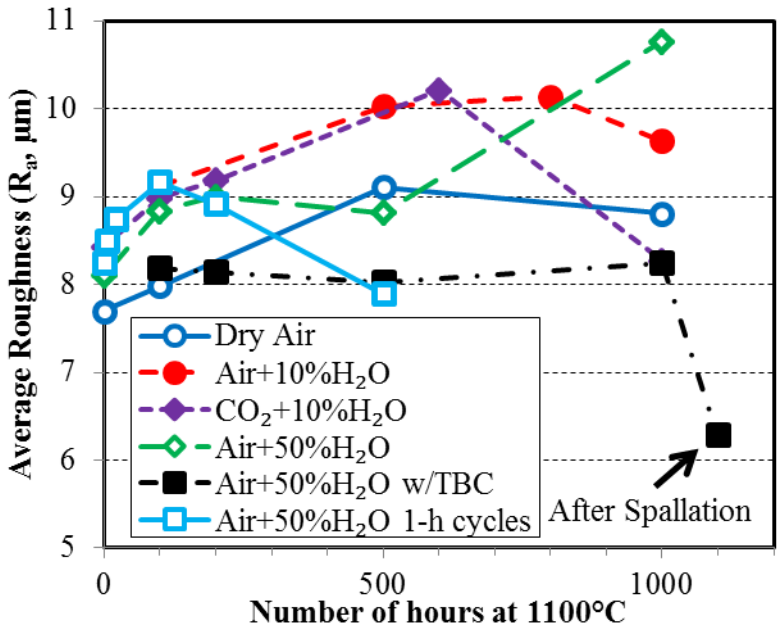
Average Roughness (R_a, µm)
11
10
9
8
7
6
5
0
500
1000
Number of hours at 1100°C
Dry Air
Air+10%H_2O
CO_2+10%H_2O
Air+50%H_2O
Air+50%H_2O w/TBC
Air+50%H_2O 1-h cycles
After Spallation

Fig. 3.

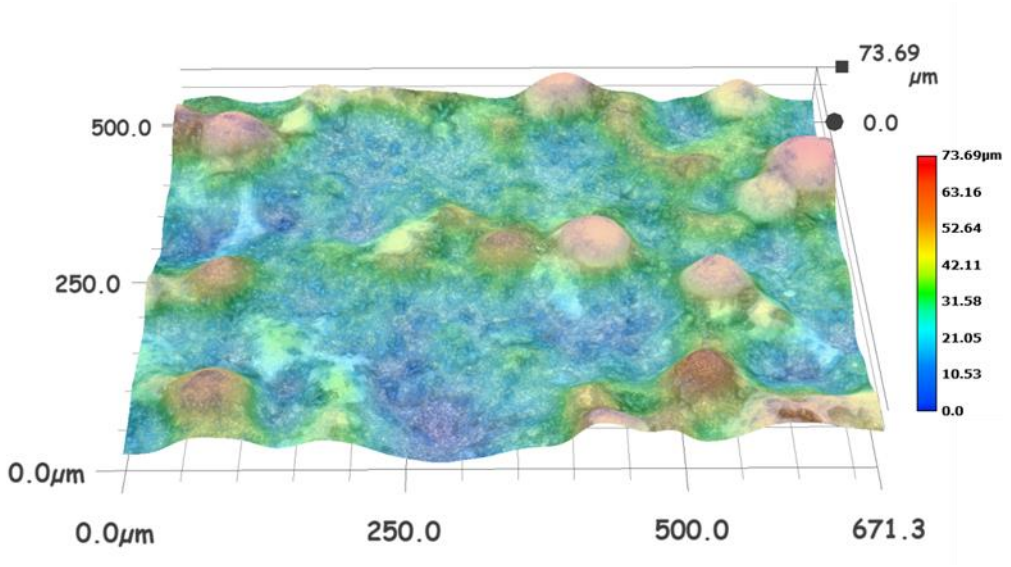
73.69
µm
0.0
500.0
250.0
0.0µm
73.69µm
63.16
52.64
42.11
31.58
21.05
10.53
0.0
0.0µm
250.0
500.0
671.3

Fig. 4.

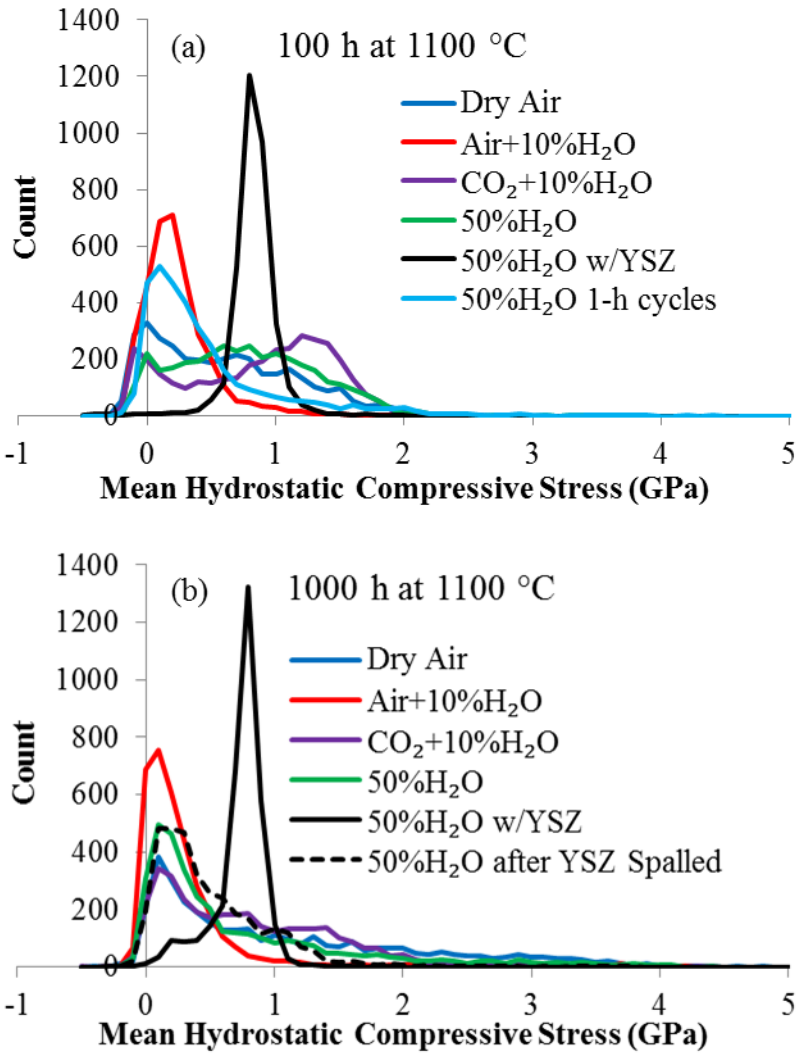
(a)
100 h at 1100 °C
Dry Air
Air+10%H2O
CO2+10%H2O
50%H2O
50%H2O w/YSZ
50%H2O 1-h cycles
Count
Mean Hydrostatic Compressive Stress (GPa)
(b)
1000 h at 1100 °C
Dry Air
Air+10%H2O
CO2+10%H2O
50%H2O
50%H2O w/YSZ
50%H2O after YSZ Spalled
Count
Mean Hydrostatic Compressive Stress (GPa)

Fig. 5.

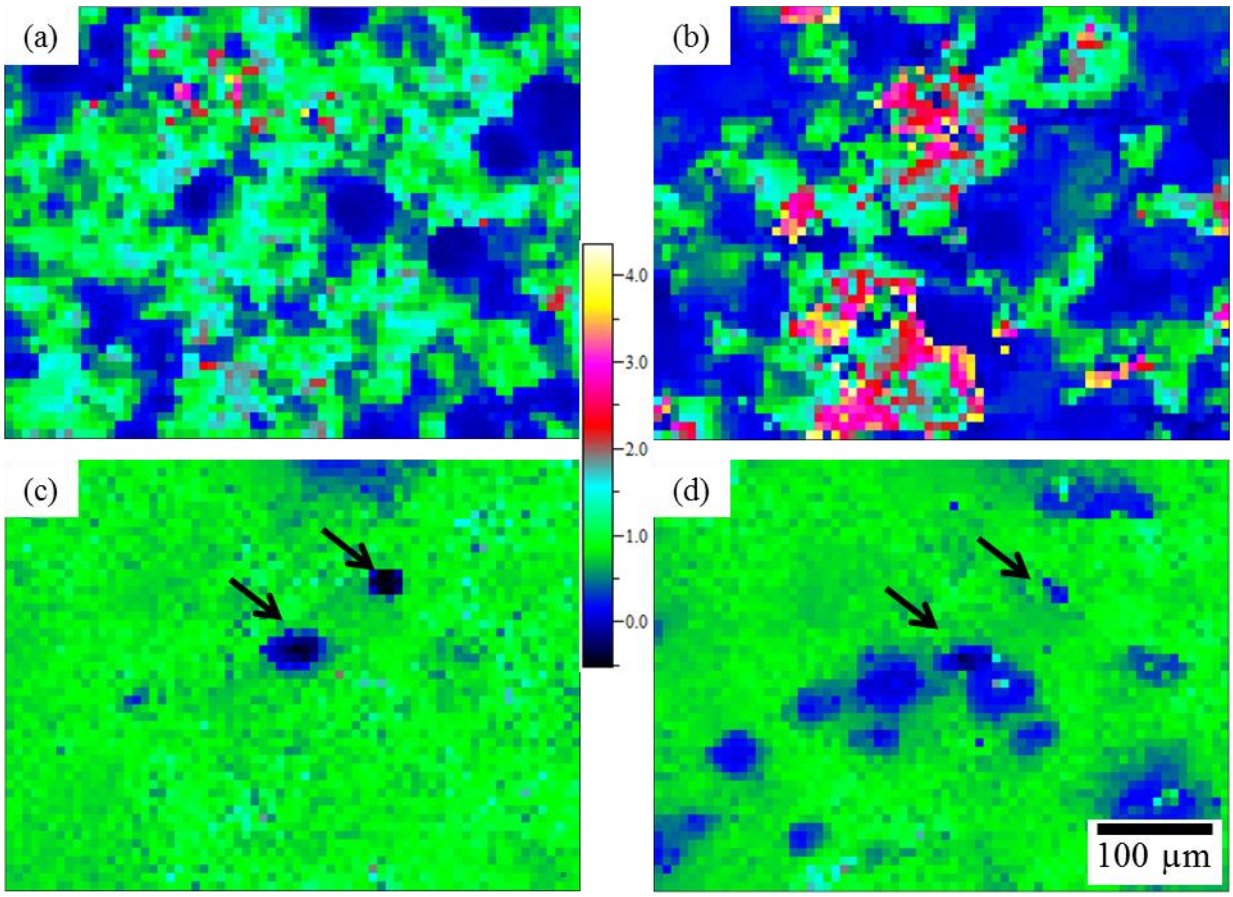

Fig. 6.

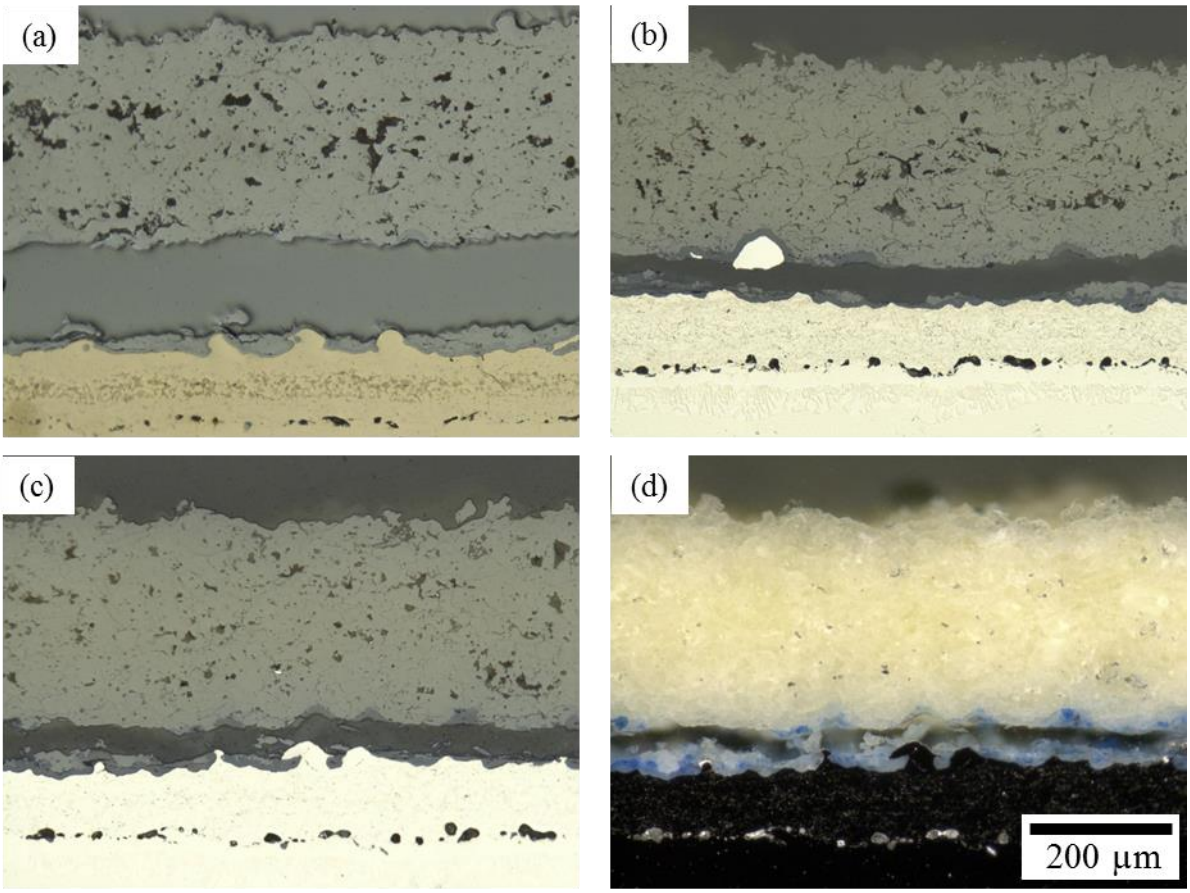

Fig. 7.

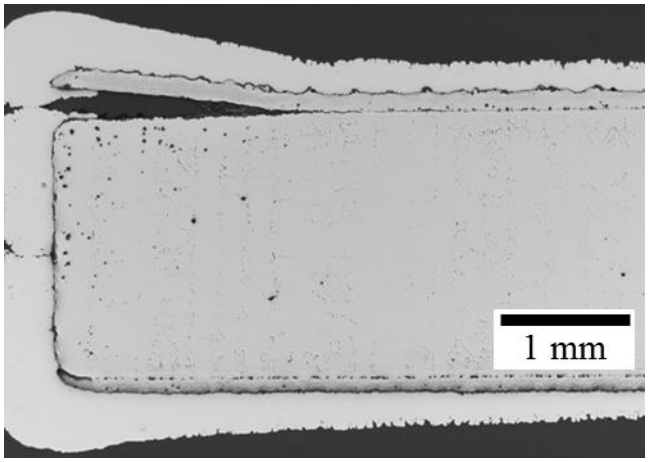

Fig. 8.

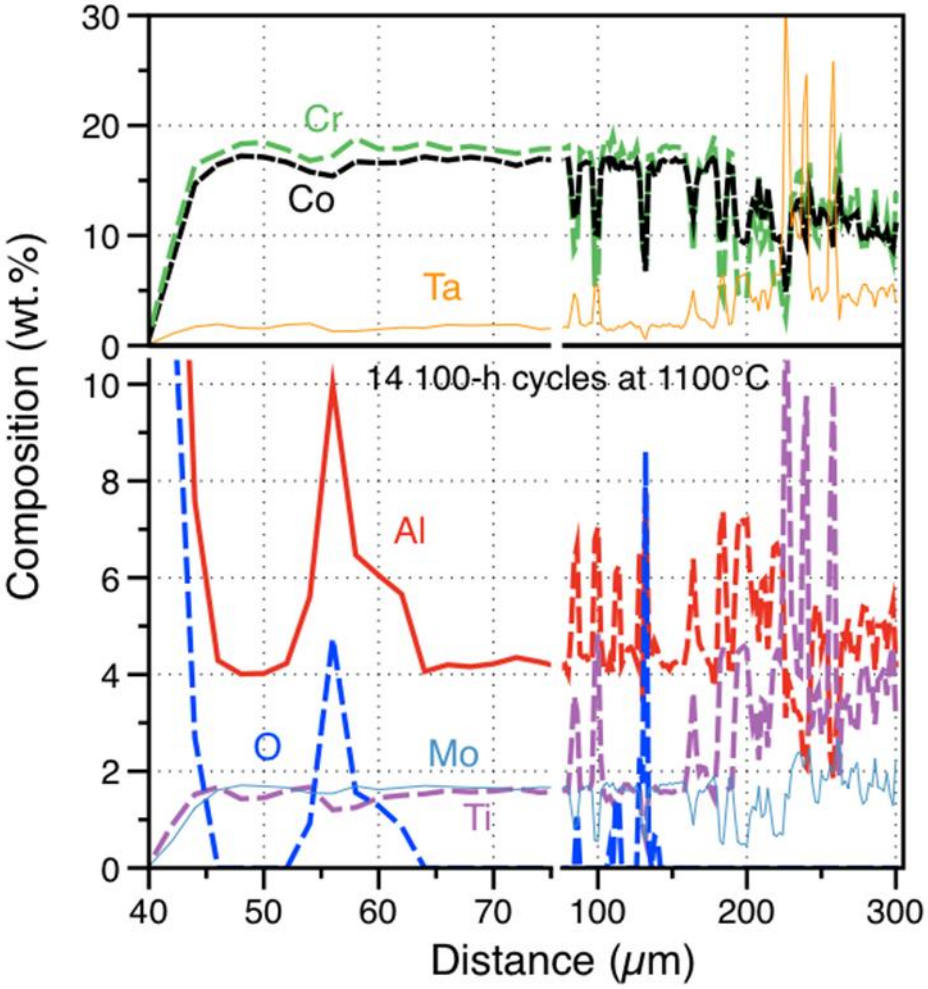
Composition (wt.%)
Distance (μm)
Cr
Co
Ta
Ti
14 100-h cycles at 1100°C
Al
O
Mo
Ti
30
20
10
0
10
8
6
4
2
0
40
50
60
70
100
200
300

Fig. 9.